Progress In Electromagnetics Research M, Vol. 63, 83–92, 2018

Design of the Permanent Magnet Linear Synchronous Motor for High Thrust and Low Cogging Force Performance

Nur A. Mohd Nasir[1, 2], Fairul Azhar[1, 2, *], Raja N. Firdaus[1, 2], Hiroyuki Wakiwaka[3], Kunihisa Tashiro[3], and Masami Nirei[4]

Abstract—Permanent magnet linear synchronous motors (PMLSM) are well known for its high thrust performance. However, such high thrust can be distorted by the existence of cogging force due to the attraction between stator core and permanent magnet (PM). To improve its performance, two parts of the PMLSM structure were considered during the design. They are PM magnetization arrangement on mover side and stator slot opening parameters on stator side. The designed models were simulated by using FEM software, and the performances of the models are then compared. The aim of the design is to achieve high thrust and low cogging force characteristics. Apart from average thrust F_{ave} and cogging force F_{cog}, the performance of the PMLSM is also evaluated using average thrust F_{ave} to cogging force ratio F_{cog}, called as thrust ratio. Based on the design, the highest thrust ratio F_{ave}: F_{cog}, obtained from radial, axial and Halbach models, are 2.5032, 2.6262 and 1.8437, respectively.

1. INTRODUCTION

Linear motor provides direct linear motion with the absence of motion translator. The absence of motion translators such as gears [1], belts and ball screws [2] reduce the motor complexity and limitation. Linear motor extensive usage in many linear motion applications also contribute by their good performances such as high speed, high accuracy and maintenance-free operation [3]. There are three types of linear motor: linear stepper motor (LSTM), linear induction motor (LIM) and linear synchronous motor (LSM). There are two major types of LSM which are switch reluctance linear synchronous motor (SRLSM) and permanent magnet linear synchronous motor (PMLSM). The existence of permanent magnet as one of the magnetic flux sources makes the PMLSM have higher thrust density [4] hence makes it perform better than the SRLSM.

The thrust of PMLSM consists of three components which are main synchronous force, reluctance force and cogging force [5]. Synchronous force is the force applied when the supply frequency (Hz) to the stator is identical to the frequency of the mover called mover speed (m/s). As the mover moves, the direction of the force and moments are relatively with the direction of the mover. Thus, the excitation frequency in any plane, lateral to the axis of the stator, is locked to the speed of motion. For this reason, they are the synchronous force and moments. Synchronous force is a function of both the input voltage and the no-load voltage induced (EMF) [6]. On the other hand, the reluctance force is define as magnetic attraction that produced as the system tries to minimize energy stored and reduces the reluctance of the magnetic path [7]. The reluctance force depends on the synchronous reactance of the d-axis, X_{sd} and q-axis, X_{sq}. In the non-salient pole motor, the synchronous reactance of the d-axis, X_{sd}

Received 19 October 2017, Accepted 17 November 2017, Scheduled 5 December 2017

* Corresponding author: Fairul Azhar bin Abdul Shukor (fairul.azhar@utem.edu.my).

[1] Faculty of Electrical Engineering, Universiti Teknikal Malaysia Melaka (UTeM), Hang Tuah Jaya, Durian Tunggal, Melaka 76100, Malaysia. [2] Electrical Machine Design, Power Electronics and Drives Research Group, CeRIA, UTeM, Hang Tuah Jaya, Durian Tunggal, Melaka 76100, Malaysia. [3] Faculty of Engineering, Shinshu University, 4-17-1 Wakasato, Nagano 380-8553, Japan. [4] Nagano National College of Technology, 716 Tokuma, Nagano 381-8550, Japan.

is almost similar to the synchronous reactance of q-axis, X_{sq} ($X_{sd} \approx X_{sq}$); therefore, reluctance force is minimized and can be neglected [6]. Cogging force in the PMLSM can be caused by the interaction between PM and the stator core of the PMLSM [8]. On the other hand, the cogging can decrease the motor efficiency, motor controllability and motor average thrust force [9]. Therefore, in designing the PMLSM, besides observing the thrust characteristics, the cogging force also needs to be considered as a part in determining the model designed with the best performance characteristics.

2. BASIC PRINCIPLE OF THE PMLSM

The PMLSM designed in this project is a cylindrical 6-slot, 8-pole type with three-phase supply. Fig. 1 shows the basic structure of the PMLSM. The PMLSM consists of six slots and a coil as stator. On the mover part, it consists of ring-shaped permanent magnets attached with a shaft. The PMLSM was designed within fixed total radius, r_{total} which is 25 mm.

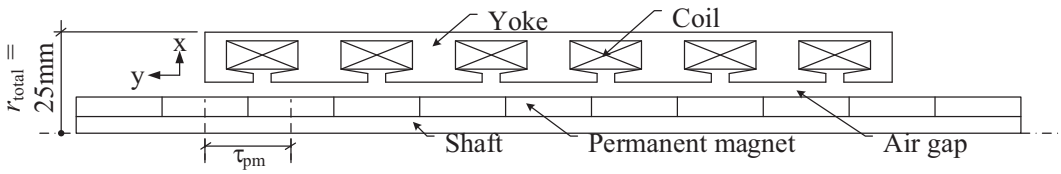

Figure 1. Axial cross section of PMLSM basic structure.

Generally, the production of thrust in the PMLSM is influenced by electrical and magnetic sources. Electrical source normally depends on current I fed to the coil. Meanwhile, for magnetic components, the thrust affected by magnetic flux density and inductance where these two elements are affected by flux of the PM and coil. The no-load rms voltage induced (EMF) E_f in one phase of armature winding by PM excitation flux is given by Equation (1) [10] where N_1 is the number of series per turn, k_w the armature winding coefficient, and Φ_f the magnetic flux produced by the PM in (Wb).

$$E_f = \pi\sqrt{2} f N_1 k_w \Phi_f \,(\text{V}) \tag{1}$$

The fundamental harmonic of the excitation magnetic flux density Φ_{f1} without armature reaction is given in Equation (2) [10] where L_i is the effective length of stator core in (mm), $\mathbf{B}_{mg1}$ the amplitude of the first harmonic of the airgap magnetic flux density in (T), and τ the pole pitch.

$$\Phi_{f1} = L_i \int_0^T \mathbf{B}_{mg1} \sin\left(\frac{\pi}{T}x\right) dx = \frac{2}{\pi}\tau L_i \mathbf{B}_{mg1} \,(\text{Wb}) \tag{2}$$

Because the armature core loss has been neglected, the electromagnetic power, P_{elm}, can be determined by the difference between the input power, P_{in}, and the armature winding loss, ΔP_{1w}. Therefore, the electromagnetic power, P_{elm}, can be expressed by Equation (3) [10] where m is the number of phase, V_1 the input voltage in volt (V), X_{sd} the d-axis armature reactance (Ω), X_{sq} the q-axis armature reactance on (Ω), and δ the load angle between V_1 and E_f. This equation is derived at the armature winding resistance, and R_1 is equal to zero.

$$P_{elm} = m\left[\frac{V_1 E_f}{X_{sd}}\sin\delta + \frac{V_1^2}{2}\left(\frac{1}{X_{sq}} - \frac{1}{X_{sd}}\right)\sin 2\delta\right] \,(\text{W}) \tag{3}$$

Equation (4) shows the electromagnetic thrust F_{dx} developed by a salient-pole PMLSM where v_s is the speed in (m/s), and by neglecting armature winding resistance the electromagnetic thrust, F_{dx} is obtained as shown in Equation (5) [10].

$$F_{dx} = \frac{P_{elm}}{v_s} \,(\text{N}) \tag{4}$$

$$F_{dx} = \frac{m}{v_s}\left[\frac{V_1 E_f}{X_{sd}}\sin\delta + \frac{V_1^2}{2}\left(\frac{1}{X_{sq}} - \frac{1}{X_{sd}}\right)\sin 2\delta\right] \,(\text{N}) \tag{5}$$

There are two components of electromagnetic thrust F_{dx} in salient pole-synchronous motor as shown in Equation (6) where F_{dxsyn} is called the synchronous thrust in (N), and F_{dxrel} is known as reluctance thrust in (N). F_{dxsyn} is the function of both input voltage V_1 and the excitation EMF E_f while F_{dxrel} depends only on input voltage V_1 and also exists in unexcited machine ($E_f = 0$) provided that d-axis synchronous reactance X_{sd} is not equal to q-axis synchronous reactance X_{sq}. However, for surface configuration of PMs $X_{sd} = X_{sq}$ (if the magnetic saturation is neglected), the electromagnetic thrust F_{dx} is given by Equation (7) [10].

$$F_{dx} = F_{dxsyn} + F_{dxrel}\,(\mathrm{N}) \tag{6}$$

$$F_{dx} \approx F_{dxsyn} = \frac{m_1}{v_2}\frac{V_1 E_f}{X_{sd}}\sin\delta\,(\mathrm{N}) \tag{7}$$

In general, it can be concluded that the electromagnetic thrust F_{dx} is influenced by input voltage V_1 and EMF E_f. Since the input voltage V_1 can be directly controlled by power supply, the design is focused on EMF E_f where it is influenced by excitation flux Φ_f.

3. DESIGN OF THE PMLSM

While the input voltage can be controlled directly by a power supply, the excitation flux Φ_f depends on the designed magnetic circuit. Previously, the PMLSM has been designed in [11]. However, the designed model has drawbacks where the produced thrust F is saturated at lower rated current due to the saturation of magnetic flux density $\mathbf{B}$ on the stator part. Therefore, the stator of PMLSM has been designed in [12] to overcome the problems. In this research, the design of the magnetic circuit is performed by designing the PM magnetization direction arrangement on the mover and slot opening parameters on the stator of the PMLSM.

Figure 2 shows the design flowchart of the PMLSM. The design of the PMLSM was started by varying the PM arrangement, and they are radial, axial and Halbach models. For each PM arrangement, the slot opening parameters, which are length of stator slot opening l_t and height of stator slot opening h_t were designed where the lowest value of the length of stator slot opening l_t and the height of stator slot opening h_t were set to 1.5 mm and 1 mm, respectively. The values of the length of stator slot opening l_t and the slot opening height h_t are then increased by 1 mm until they reached their respective limit values. The designed PMLSM models were simulated by using FEM software, and the performances were evaluated and compared. Based on the performance, the best model was chosen.

3.1. Variation of PM Arrangement on Mover Side

There are three types of PM arrangement set in this paper. They are radial [13], axial [14] and Halbach [15]. Fig. 3 shows the three types of PM arrangement. Besides that, in order to make valid comparison, the PM pitch τ_{pm} and radius r_{pm} were maintained to all the three of PM arrangement in order to make a valid comparison of their performances. Therefore, PM width w_{pm} for each PM arrangement is changed accordingly as shown in Table 1.

Table 1. Permanent magnet dimensions.

PM arrangements	PM width, w_{pm} (mm)	PM radius, r_{pm} (mm)	PM pitch, τ_{pm} (mm)	Shaft material
Radial	6	7	12	Ferromagnetic (SS400)
Axial	6	7	12	Non-ferromagnetic
Halbach	12	7	12	Non-ferromagnetic

Each PM arrangement has a different configuration where Halbach array has more complex arrangement than radial and axial arrays. Halbach array is basically a combination of radial and axial arrays [16]. Apart from differences in magnetization direction arrangement, the material used is

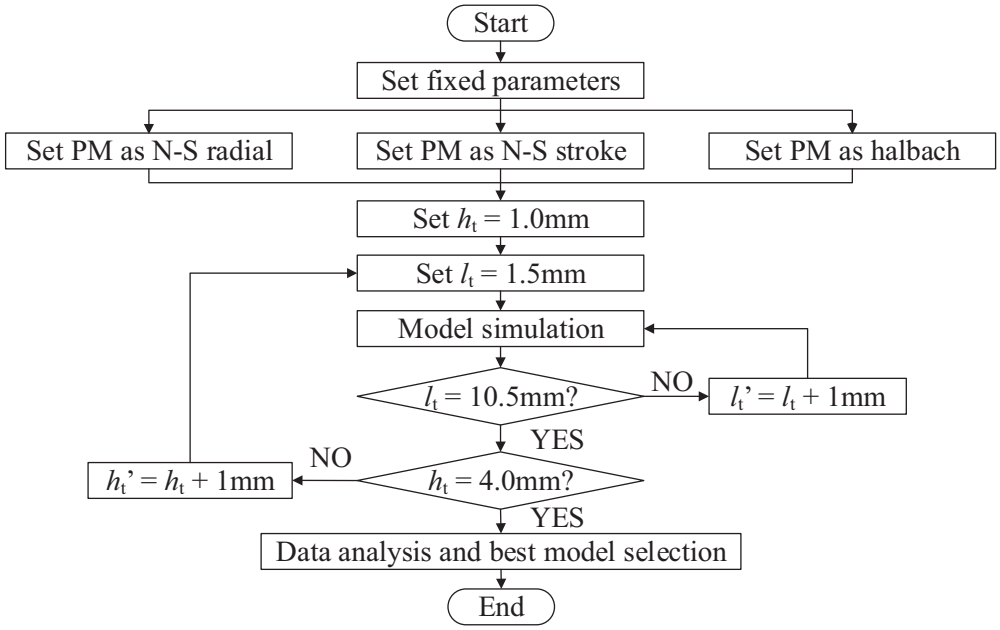

Figure 2. The PMLSM design flowchart.

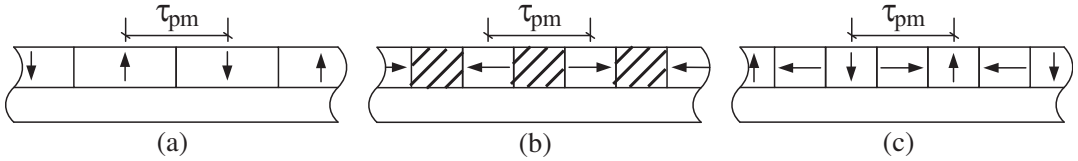

Figure 3. The three different PM arrangement; (a) radial, (b) axial, (c) Halbach.

also a bit different in order to optimize the flux path, flux leakage and magnetic flux density for each PM arrangement. Due to this fact, different shaft materials are used for different PM arrangements where a ferromagnetic shaft is used in radial array while both axial and Halbach arrays use a non-ferromagnetic shaft to reduce flux leakage. Besides, the axial array requires ferromagnetic spacer added between adjacent PMs. The ferromagnetic spacer is needed for flux conducting area hence increases magnetic flux density **B** produced by the PM. However, radial and Halbach arrays do not require any ferromagnetic spacer for flux path.

3.2. Design of Stator Slot Opening Parameters

There are two parameters of stator slot opening designed, which are slot opening length l_t and slot opening height h_t. The position of the slot opening parameters is shown in Fig. 4. Apart from the slot opening parameters, the other PMLSM structure parameters, such as airgap length δ and coil pitch τ_c, were fixed and as listed in Table 2. The variations of stator slot opening parameters were applied to the three types of PM arrangement.

During designing slot opening parameters, the values of slot opening length l_t and slot opening height h_t were varied starting from the lowest possible value and increased by 1 mm until they reached maximum possible value. Table 2 lists the range of stator slot opening parameters. The limit of slot opening's height depends on the value of lower stator yoke thickness t_{y2} which is 3 mm, whereas the limit of slot opening's length is determined by the value of coil width w_c where in this case, the coil width w_c is 10 mm. All the models were then simulated, and the performances obtained were compared. These parameters were determined based on the previous stage of the PMLSM stator designed in [12].

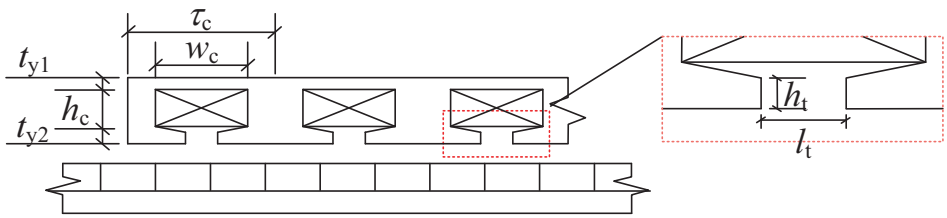

Figure 4. PMLSM stator slot opening parameters.

Table 2. PMLSM structure parameters.

Structure parameters	Value
Total outer radius, r_{total} (mm)	25
Coil pitch, τ_c (mm)	16
Permanent magnet pitch, τ_{pm} (mm)	12
Permanent magnet outer radius, r_{pm} (mm)	13
Shaft radius, r_s (mm)	6
Lower yoke thickness, t_{y2} (mm)	3
Upper yoke thickness, t_{y1} (mm)	2
Air gap length, δ (mm)	0.5
Coil resistance (per coil), R (Ω)	6.93
Coil turn (per coil), N	220
Length of slot opening, l_t (mm)	$1.5 \sim 9.5$
Height of slot opening, h_t (mm)	$1 \sim 3$

4. PERFORMANCE COMPARISON OF THE PMLSM

All the designed PMLSM models were simulated by using FEM software. Based on the obtained result, the performances of the PMLSM were observed and compared. Three performances of the PMLSM are compared. They are average thrust F_{ave}, cogging force F_{cog}, and ratio of average thrust to cogging force F_{ave}: F_{cog} or called as thrust ratio.

4.1. Comparison of Average Thrust, $\mathbf{F_{ave}}$

Generally, the performances of the PMLSM are evaluated based on thrust characteristics [17]. Therefore, all the PMLSM models with different slot opening parameters and PM magnetization direction arrangements are evaluated based on the thrust characteristics. Fig. 5 shows the sample of thrust for three different PM arrangements of the PMLSM. To evaluate the thrust F at certain current I value, the average thrust F_{ave} is used. Therefore, based on thrust F characteristics obtained as Fig. 5, the average thrust F_{ave} is calculated using Equation (8).

$$F_{\text{ave}} = \frac{1}{x_T} \int_0^x F dx \,(\text{N}) \tag{8}$$

where F_{ave} is the average thrust in (N), F the thrust in (N), and x and x_{T} are the instantaneous and maximum displacements, respectively in (m).

Principally, the models were injected with the current I started from 0.5 A to 3 A with 0.5 A increment. However, the result is taken at the rated current in order to evaluate the thrust performance at its rated value. The average thrust F_{ave} is calculated, and the data are tabulated and presented in Fig. 6. Based on Fig. 6, it is shown that both radial and axial models produce a similar pattern of average thrust F_{ave}, as shown in Fig. 6(a) and Fig. 6(b). Compared to radial and axial ones, Halbach models produce a different pattern of average thrust as shown in Fig. 6(c). Fig. 6(c) shows that the

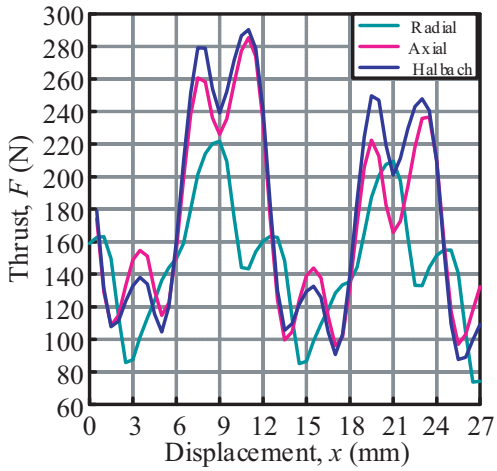

Figure 5. Thrust, F at 3 A.

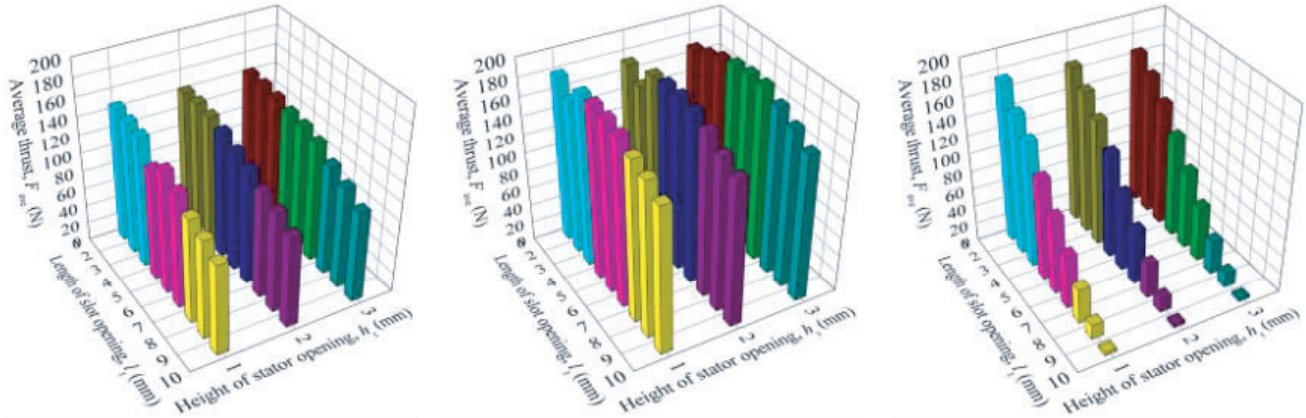

(a) (b) (c)

Figure 6. PMLSM average thrust, F_{ave} at 3 A; (a) radial, (b) axial, (c) Halbach.

average thrust produced by Halbach models decreases as the length of stator slot opening l_t increases. Oppositely, the average thrust F_{ave} produced by radial and axial models does not show a lot of changes over the changes of stator slot opening parameters.

Basically, the height of stator slot opening h_t for each variation of the length of stator slot opening l_t does not give any significant difference towards thrust characteristics. This can be observed in Fig. 6 where Figs. 6(a), (b) and Fig. 6(c) show the thrust characteristics of the radial, axial and Halbach models, respectively. It is shown that the thrust produced by the same length of stator slot opening l_t with different heights of stator slot opening h_t is almost constant with a small amount of differences.

Based on average thrust presented in Fig. 6, the model that produced highest average thrust, F_{ave}, on each PM arrangement was determined and compared in Table 3. Table 3 shows that the axial model with $l_t = 5.5$ mm and $h_t = 2$ mm has the highest average thrust which is 189 N. Meanwhile, for both radial and Halbach arrays, the highest average thrust is produced by the models with $l_t = 1.5$ mm and $h_t = 1$ mm. The average produced thrusts are 145 N and 176 N, respectively.

4.2. Comparison of Cogging Force, $\mathbf{F_{cog}}$

Apart from thrust F, the effect of stator slot opening parameters and PM arrangement variations are also evaluated based on the performance of cogging force, F_{cog}. Fig. 7 shows the cogging force F_{cog} characteristics for three PM arrangements for the variation of all the slot opening parameters.

Table 3. Maximum average thrust for different PM arrangement.

PM arrangement	Highest average thrust, $F_{\text{ave,rated}}$ (N)	Length of slot opening, l_t (mm)	Height of slot opening, h_t (mm)
Radial	145	1.5	1
Axial	189	5.5	2
Halbach	176	1.5	1

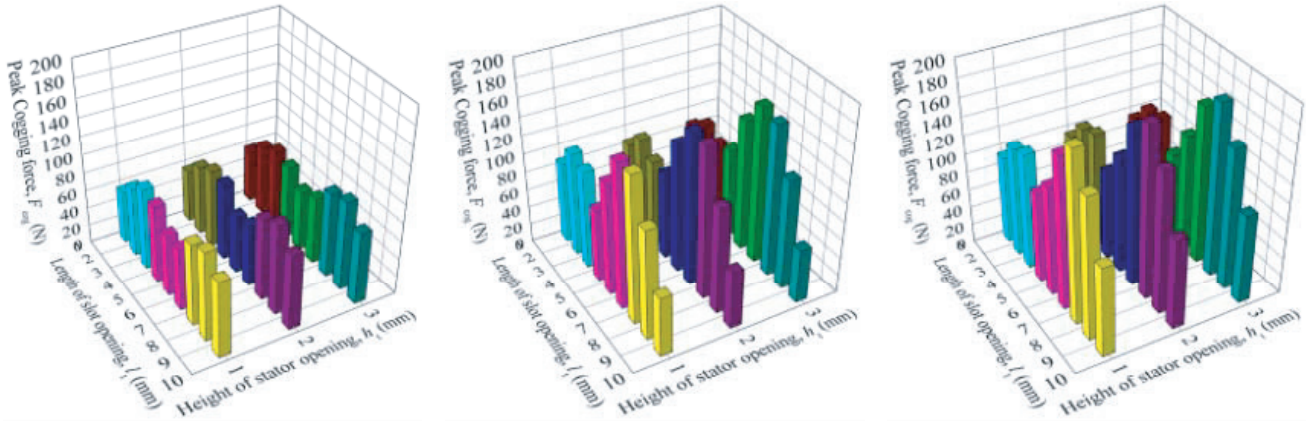

Figure 7. PMLSM cogging force, F_{cog}; (a) radial, (b) axial, (c) Halbach.

Based on Fig. 7, it is shown that overall radial models produce lower cogging force F_{cog} than axial and Halbach models. The cogging force F_{cog} characteristics of the radial models do not have much differences as the length of stator slot opening l_t increases, and the value is almost similar. Meanwhile, compared to Halbach models, axial models produced lower cogging force, F_{cog}. Compared to radial, axial models show a large fluctuation of cogging force F_{cog} with variation of the length of stator slot opening l_t, and this can be observed in Fig. 7(b). Similar to axial models, the Halbach models also show a significant change of cogging force F_{cog}, as the length of stator slot opening l_t is varied as shown in Fig. 7(c).

Similar to thrust F characteristics as discussed previously, the variation of the height of stator slot opening h_t does not give any substantial effect towards the characteristics of cogging force F_{cog} with the same length of stator slot opening l_t, as shown in Fig. 7. This can be seen in Fig. 7(a) and Fig. 7(c) for radial and Halbach models, respectively. The differences are quite small, and the value of cogging force F_{cog} is almost constant for the height of stator slot opening, h_t, models with the same length of stator slot opening, l_t. However, some models in axial array show that the value of cogging force F_{cog} shows significant differences as shown in Fig. 7(b). Fig. 7(b) shows that axial $l_t = 2.5\,\text{mm}$, $3.5\,\text{mm}$, $4.5\,\text{mm}$, and $5.5\,\text{mm}$ has big differences for different heights of stator slot opening, h_t.

Based on Fig. 7(a), the radial models with the lowest and highest cogging forces were identified. The lowest cogging of the radial arrangement is produced by the model with $l_t = 1.5\,\text{mm}$ and $h_t = 2\,\text{mm}$ which is 57 N while the model with $l_t = 8.5\,\text{mm}$ and $h_t = 2\,\text{mm}$ produced the highest cogging which is 100 N. Meanwhile, axial model with $l_t = 8.5\,\text{mm}$ and $h_t = 2\,\text{mm}$ produced the highest cogging which is 169 N while the axial model with $l_t = 9.5\,\text{mm}$ and $h_t = 3\,\text{mm}$ produced the lowest cogging which is 60 N. The cogging force characteristic of the axial model is shown in Fig. 7(b). Fig. 7(c) shows the cogging force characteristic for the Halbach models. From Fig. 7(c), the Halbach model with $l_t = 7.5\,\text{mm}$ and $h_t = 3\,\text{mm}$ is identified to produce the highest cogging which is 186 N while the Halbach model with $l_t = 4.5\,\text{mm}$ and $h_t = 3\,\text{mm}$ produced the lowest cogging which is 93 N.

Table 4 lists the model with the lowest cogging force F_{cog} for three PM arrangements. Table 4

Table 4. The lowest cogging force for different PM arrangement.

PM arrangement	Lowest cogging force, $F_{\text{cog,min}}$ (N)	Length of slot opening, l_t (mm)	Height of slot opening, h_t (mm)
Radial	57	1.5	1
Axial	60	9.5	3
Halbach	93	4.5	3

summarizes that the radial model with $l_t = 1.5$ mm and $h_t = 1$ mm produced lower cogging force F_{cog} than other PM arrangement models, which is 57 N. Meanwhile, the axial model with $l_t = 5.5$ mm and $h_t = 2$ mm has the cogging force F_{cog} a bit higher than the radial model but much lower than the Halbach model which is 60 N where the cogging force F_{cog} for the Halbach model is 93 N.

4.3. Ratio of Average Thrust to Cogging Force, $\mathbf{F_{ave}}$: $\mathbf{F_{cog}}$

Based on the average thrust and cogging force characteristics, the ratios of thrust to cogging force were calculated and presented in the form of contour plot as shown in Fig. 8. The purpose of finding thrust to cogging force ratio is to identify the models with optimum thrust performance from each PM arrangement. High thrust ratio means that the model has high thrust with low cogging force while low thrust ratio indicates low thrust with high cogging force. Fig. 8 shows that the red region is for high ratio while blue region indicates the area for low ratio.

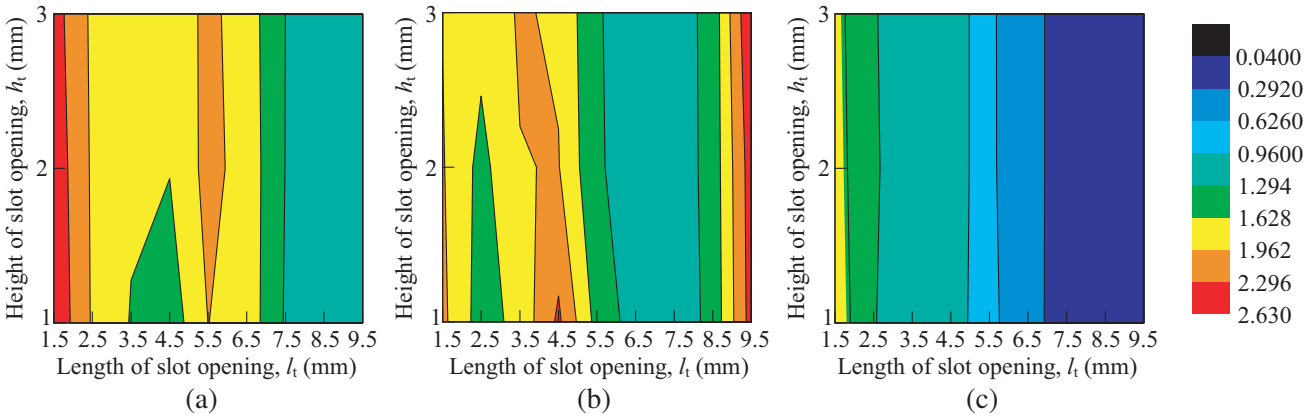

Figure 8. Ratio of average thrust, F_{ave} to cogging force, F_{cog}; (a) radial, (b) axial, (c) Halbach.

Compared to radial and Halbach models, the thrust ratio F_{ave}: F_{cog} characteristics of axial models do not change uniformly as the length of slot opening l_t and height of slot opening h_t are varied. These characteristics can be seen in Fig. 8(b). In a certain value of the length of slot opening l_t, the values of thrust ratio for the different heights of slot opening, h_t, differ significantly. This can be seen from the models with $l_t = 1.5$ mm, $l_t = 2.5$ mm and $l_t = 4.5$ mm. Similar to radial model, the highest range of thrust ratio is indicated by the red region between 2.2960 and 2.6300 where the model with the highest thrust ratio has the thrust ratio of 2.6262. The model is axial with $l_t = 9.5$ mm and $h_t = 3$ mm. Meanwhile, the models with $l_t = 6.5$ mm and $l_t = 7.5$ mm fall under the region of low thrust ratio range which is 0.9600 to 1.2940. Specifically, the axial model with the lowest thrust ratio is the model with $l_t = 9.5$ mm and $l_t = 4.5$ mm with the thrust ratio of 1.0807.

Based on the Halbach average thrust F_{ave} and cogging force F_{cog} characteristics discussed previously, it is shown that the average thrust of Halbach array decreased as the length of slot opening l_t increased while cogging force generally increased as the length of slot opening l_t decreased. Therefore, the thrust

ratio F_{ave}: F_{cog} of Halbach models decreased as the length of slot opening l_t increased. On the other hand, the thrust ratio does not affect much by the variation of the height of slot opening, h_t. Fig. 8(c) shows the thrust ratio F_{ave}: F_{cog} contour plot for the Halbach models where it is shown that the highest thrust ratio F_{ave}: F_{cog} produced by the Halbach models is significantly lower than both radial and axial models in which the range of highest thrust ratio falls between 1.628 and 1.962. Similarly, the lowest thrust ratio F_{ave}: F_{cog} is also low which is in the range of 0.0400 to 0.2920. The highest thrust ratio F_{ave}: F_{cog} of the Halbach produced by the model with $l_t = 1.5\,\text{mm}$ and $h_t = 1\,\text{mm}$ is at the ratio of 1.8439. Meanwhile, the Halbach model with $l_t = 9.5\,\text{mm}$ and $h_t = 2\,\text{mm}$ has the lowest thrust ratio F_{ave}: F_{cog}, which is 0.0364.

Table 5 shows the comparison of maximum thrust ratios produced by the models from these PM arrangements. From Table 5, it can be summarized that axial model has the highest thrust ratio which is 2.6262 with average thrust F_{ave} of 159 N and cogging force F_{cog} of 60 N. Radial model has a thrust ratio lower than axial model but higher than Halbach model which is 2.5032. The radial model has the average thrust F_{ave} of 148 N and cogging force F_{cog} of 57 N. Halbach model has the lowest thrust ratio which is 1.8439 with average thrust F_{ave} of 176 N and cogging force F_{cog} of 95 N. Based on the thrust ratio, it is shown that, though Halbach model produced the highest average thrust F_{ave}, the cogging force F_{cog} was also high hence resulted in low thrust ratio.

Table 5. Maximum thrust ratio for different PM arrangement.

PM arrangement	Thrust ratio, F_{ave}: F_{cog}	Average thrust, F_{ave} (N)	Cogging force, F_{cog} (N)	Length of slot opening, l_t (mm)	Height of slot opening, h_t (mm)
Radial	2.5032	148	57	1.5	1
Axial	2.6262	159	60	9.5	3
Halbach	1.8439	176	95	1.5	1

5. CONCLUSION

A PMLSM is designed in this paper. The design of PMLSM consists of two parts. The first part is to vary the PM arrangement, and the second part is to vary the stator slot opening parameters. There are three different PM arrangements which are radial, axial and Halbach models while the two parameters of the stator slot opening are the length of stator slot opening l_t and the height of stator slot opening h_t. For each PM arrangement, the length of stator slot opening l_t and the height of stator slot opening h_t were set to their minimum values which are 1.5 mm and 1 mm, respectively. The values of the length of stator slot opening l_t and the slot opening height h_t are then increased by 1 mm until they reach their respective limit values. All the models designed were simulated by using FEM software, and the results obtained were compared and evaluated. There are three performances evaluated in this paper which are average thrust, cogging force and thrust ratio. These performance evaluations are used to determine the models with the optimum performances. Based on average thrust and cogging force characteristics, the ratio between these two performances is determined. Radial model with $l_t = 1.5\,\text{mm}$ and $h_t = 1\,\text{mm}$ has the highest thrust ratio, F_{ave}: F_{cog}, which is 2.5032, and the highest thrust ratio, F_{ave}: F_{cog}, of axial model is $l_t = 9.5\,\text{mm}$ and $h_t = 3\,\text{mm}$ which is 2.6262. Meanwhile, with the ratio of 1.8439, Halbach model with $l_t = 1.5\,\text{mm}$ and $h_t = 1\,\text{mm}$ produced the highest thrust ratio, F_{ave}: F_{cog}. However, as the thrust F is considered as the main factor in evaluating PMLSM performances, the Halbach model with $l_t = 1.5\,\text{mm}$ and $h_t = 1\,\text{mm}$ has been chosen as the best final model. This model has the highest average thrust, F_{ave}, which is 176 N.

ACKNOWLEDGMENT

The authors would like to thank Ministry of Education & Universiti Teknikal Malaysia Melaka (UTeM) for providing PJP/2016/FKE/HI5/S01478.

REFERENCES

1. Pakdelian, S., Y. Deshpande, and H. A. Toliyat, "An electric machine integrated with trans-rotary magnetic gear," *2012 IEEE Energy Conversion Congress and Exposition (ECCE)*, 3356–3362, Raleigh, NC, 2012.
2. Brando, G., A. Dannier, A. Del Pizzo, and L. P. Di Noia, "Electric steering for aircraft nose landing gears using axial-flux permanent-magnet motors," *2016 XXII International Conference on Electrical Machines (ICEM)*, 761–767, Lausanne, 2016.
3. Varaticeanu, B. D. and P. Minciunescu, "Modelling and analysis of dual-sided coreless linear synchronous motor," *Rev. Roum. Sci. Tech., Electrotech Net Energy*, 2, Bucarest, 2014.
4. Oshima, S., S. Tahara, and K. Tagawa, "Thrust and thrust ripple of linear reluctance motor compared to permanent linear synchronous motor," *15th International Conference on Electrical Machine and Systems (ICEMS)*, 1–4, 2012.
5. He, Q. and X. Bao, "Reducing cogging torque in permanent-magnet synchronous motors by auxiliary teeth method," *2016 IEEE 11th Conference on Industrial Electronics and Applications (ICIEA)*, 1488–1495, Hefei, 2016.
6. Friswell, M. I., *Dynamics of Rotating Machines*, 228, Cambridge University Press, 2010.
7. Tzou, H. and T. Fukuda, *Precision Sensors, Actuators and Systems*, 75, Springer Science and Business Media, 2012.
8. Li, B., J. Zhao, X. Liu, Y. Guo, H. Hu, and J. Li, "Detent force reduction of an arc-linear permanent-magnet synchronous motor by using compensation windings," *IEEE Transactions on Industrial Electronics*, Vol. 64, No. 4, 3001–3011, 2017.
9. Patel, A. N., "Influence of stator teeth shaping on cogging torque of radial flux permanent magnet brushless DC motor," *2016 Biennial International Conference on Power and Energy Systems: Towards Sustainable Energy (PESTSE)*, 1–4, 2016.
10. Gieras, J. F. and Z. J. Piech, *Linear Synchronous Motor-Transportation and Automation Systems*, CRC Press, Boca Raton, Florida, 2000.
11. Azhar, F., H. Wakiwaka, K. Tashiro, and M. Nirei, "Design and performance index comparison of the permanent magnet linear motor," *Progress In Electromagnetics Research M*, Vol. 43, 101–108, 2015.
12. Mohd Nasir, N. A., F. A. Abdul Shukor, R. N. F. K. Raja Othman, H. Wakiwaka, and K. Tashiro, "Design of permanent magnet linear synchronous motor stator to improve magnetic flux density profile toward high thrust density performance," Mohamed Ali M., Wahid H., Mohd Subha N., Sahlan S., Md. Yunus M., Wahap A. (eds.), *Modeling, Design and Simulation of Systems, AsiaSim 2017, Communications in Computer and Information Science*, Vol. 751, Springer, Singapore, 2017.
13. Ling, Z., J. Ji, J. Wang, and W. Zhao, "Design optimization and test of a radially magnetized magnetic screw with discretized PMs," *IEEE Trans. on Industrial Electronics*, No. 99, 1-1, 2017.
14. Shi, W., C. Xiao, Y. Lei, B. Yu, F. Wu, and P. Zheng, "Optimization on thrust ripple of an axial-flux permanent-magnet linear synchronous machine," *2011 International Conference on Electrical Machines and Systems*, 1–6, Beijing, 2011.
15. Shahosseini, I. and K. Najafi, "Cylindrical halbach magnet array for electromagnetic vibration energy harvesters," *2015 28th IEEE International Conference on Micro Electro Mechanical Systems (MEMS)*, 1051–1054, Estoril, 2015.
16. Koo, M. M., J. Y. Choi, H. J. Shin, and J. M. Kim, "No-load analysis of PMLSM with halbach array and PM overhang based on three-dimensional analytical method," *IEEE Transactions on Applied Superconductivity*, Vol. 26, No. 4, 1–5, 2016.
17. Azhar, F., N. A. M. Nasir, R. N. Firdaus, H. Wakiwaka, K. Tashiro, and M. Nirei, "Comparison and prediction of performance index of permanent magnet linear motor," *2016 IEEE International Conference on Power and Energy (PECon)*, 558–563, 2016.